Eur. Phys. J. C 56, 57–62 (2008)
DOI 10.1140/epjc/s10052-008-0629-z

THE EUROPEAN PHYSICAL JOURNAL C

Regular Article – Theoretical Physics

Unified model for small-t and high-t scattering at high energies: predictions at RHIC and LHC

E. Martynov[1], B. Nicolescu[2,a]

[1] N.N. Bogolyubov Institute for Theoretical Physics, National Academy of Sciences of Ukraine, Kiev, Ukraine
[2] Theory Group, Laboratoire de Physique Nucléaire et des Hautes Énergies (LPNHE)[b], CNRS and Université Pierre et Marie Curie, 4 Place Jussieu, 75005 Paris, France

Received: 14 February 2008 / Revised version: 20 March 2008 /
Published online: 4 June 2008 –

Abstract. The urgency of predictions in the large-t region at LHC stimulated us to present a unified model of small- and high-t scattering at high energies. Our model is based on safe theoretical ground: analyticity, unitarity, Regge behavior, gluon exchange and saturation of bounds established in axiomatic quantum field theory. We make precise predictions for the behavior of the differential cross sections at high t, the evolution of the dip–shoulder structure localized in the region $0.5 \lesssim |t| \lesssim 0.8\,\mathrm{GeV}^2$ and the radical violation of the exponential behavior of the first diffraction cone at small t.

PACS. 12.40.Nn; 13.75.Cs; 13.85.Dz; 13.85.Lg

Avila, Gauron and Nicolescu (AGN) recently published a good fit of forward and non-forward data in pp and $\bar{p}p$ scattering, leading to intriguing predictions at RHIC and LHC [1, 2].

The AGN model was defined to be valid only at moderate t values ($0 \leq |t| \leq 2.6\,\mathrm{GeV}^2$). We stress that this model is based on safe theoretical ground: analyticity, unitarity, Regge behavior and saturation of bounds established in axiomatic quantum field theory.

In the present paper we generalize this model by extending its validity to high-t values ($0 \leq |t| \leq 16\,\mathrm{GeV}^2$), and we present our predictions at RHIC and LHC. Such predictions are urgently needed in view of the near start of experiments at LHC.

As data we used the dataset recently proposed by Cudell, Lengyel and Martynov (CLM), who built a coherent dataset of all existing data for $5 \leq \sqrt{s} \leq 1800\,\mathrm{GeV}$ and $0 \leq |t| \leq 16\,\mathrm{GeV}^2$[3]. The raw data are, of course, contained in the Durham database [4], but CLM introduced a detailed study of the systematic errors and gathered into a common format more than 260 subsets of data from more than 80 experimental papers. The CLM can be considered as a *standard dataset*, which is available online [5].

Let us first define the even-under-crossing and the odd-under-crossing amplitudes $F_{\pm}(s,t)$:

$$F_{\pm} = \frac{1}{2}(F_{pp}(s,t) \pm F_{\bar{p}p}(s,t))\,, \tag{1}$$

which are normalized so that

$$\sigma_t(s) = \frac{1}{\sqrt{s(s-4m_p^2)}}\,\mathrm{Im}\,F(s,t=0)\,,$$
$$\rho(s) = \frac{\mathrm{Re}\,F(s,t=0)}{\mathrm{Im}\,F(s,t=0)}\,, \tag{2}$$
$$\frac{\mathrm{d}\sigma}{\mathrm{d}t}(s,t) = \frac{1}{16\pi g s(s-4m_p^2)}|F(s,t)|^2\,,$$
$$g = 0.3893797\,\mathrm{mb\,GeV}^{-2}\,, \tag{3}$$

m_p being the mass of the proton.

In the AGN model[1] $F_+(s,t)$ is defined as a superposition of the following contributions: the Froissaron $F_+^H(s,t)$, the pomeron pole $F_+^P(s,t)$, the pomeron–pomeron Regge cut $F_+^{PP}(s,t)$, the secondary $f_2 - a_2$ reggeon $F_+^R(s,t)$ and the reggeon–pomeron cut $F_+^{RP}(s,t)$:

$$F_+(s,t) = F_+^H(s,t) + F_+^P(s,t) + F_+^{PP}(s,t) + F_+^R(s,t) + F_+^{RP}(s,t)\,, \tag{4}$$

where

$$F_+^H(s,t) = \mathrm{i}s\Big\{H_1 \ln^2\tilde{s}\frac{2J_1(K_+\tilde{\tau})}{K_+\tilde{\tau}}\exp(b_{+1}t) + H_2\ln\tilde{s}J_0(K_+\tilde{\tau})\ln\tilde{s}\exp(b_{+2}t) + H_3[J_0(K_+\tilde{\tau}) - K_+\tilde{\tau}J_1(K_+\tilde{\tau})]\exp(b_{+3}t)\Big\}\,, \tag{5}$$

[a] e-mail: nicolesc@lpnhe.in2p3.fr
[b] Unité de Recherche des Universités Paris 6 et Paris 7, associée au CNRS

[1] The notation for the signature factors differs from the one of the original AGN model.

$$F_+^P(s,t) = C_P \exp(b_P t) \times \Phi_+(\alpha_P(t))(s/s_0)^{\alpha_P(t)}\,, \quad (6)$$

$$F_+^{PP}(s,t) = \frac{C_{PP}}{\ln\tilde{s}} \exp(b_{PP} t) \times \Phi_+(\alpha_{PP}(t))(s/s_0)^{\alpha_{PP}(t)}\,, \quad (7)$$

$$F_+^R(s,t) = C_R^+ \exp(b_R^+ t) \times \Phi_+(\alpha_R^+(t))(s/s_0)^{\alpha_R^+(t)}\,, \quad (8)$$

$$F_+^{RP}(s,t) = \frac{-\mathrm{i}tC_{RP}^+}{\ln\tilde{s}} \exp(b_{RP}^+ t) \times \Phi_+(\alpha_{RP}^+(t))(s/s_0)^{\alpha_{RP}^+(t)}\,, \quad (9)$$

$$\tilde{s} = (s/s_0)\exp\left(-\frac{1}{2}\mathrm{i}\pi\right), \quad s_0 = 1\,\mathrm{GeV}^2\,, \quad (10)$$

$$\tilde{\tau} = \sqrt{-t/t_0}\ln\tilde{s}\,, \quad t_0 = 1\,\mathrm{GeV}^2\,, \quad (11)$$

$$\Phi_+(\alpha(t)) = \mathrm{i}\sin\left(\frac{\pi}{2}\alpha(t)\right) - \cos\left(\frac{\pi}{2}\alpha(t)\right), \quad (12)$$

$$\alpha_P(t) = 1 + \alpha_P' t\,, \quad (13)$$

$$\alpha_{PP}(t) = 1 + \alpha_P' t/2\,, \quad (14)$$

$$\alpha_R^+(t) = \alpha_R^+(0) + \alpha_R^{+\prime} t\,, \quad (15)$$

$$\alpha_{RP}^+(t) = \alpha_R^+(0) + \frac{\alpha_P'\alpha_R^{+\prime}}{\alpha_P' + \alpha_R^{+\prime}} t\,, \quad (16)$$

H_1, H_2, H_3, K_+, b_{+1}, b_{+2}, b_{+3}, C_P, b_P, C_{PP}, b_{PP}, C_R^+, b_{RP}^+, C_{RP}^+, b_{RP}^+, α_P', $\alpha_R^+(0)$ and $\alpha_R^{+\prime}$ being constants. J_0 and J_1 are Bessel functions.

In its turn, $F_-(s,t)$ is defined, in the AGN model, as a superposition of the maximal odderon contribution $F_-^{MO}(s,t)$, the odderon pole $F_-^O(s,t)$, the odderon–pomeron cut $F_-^{OP}(s,t)$, the secondary ρ–ω reggeon $F_-^R(s,t)$ and the reggeon–pomeron cut $F_-^{RP}(s,t)$:

$$F_-(s,t) = F_-^{MO} + F_-^O(s,t) + F_-^{OP}(s,t) + F_-^R(s,t) + F_-^{RP}(s,t)\,, \quad (17)$$

where

$$F_-^{MO}(s,t) = s\Big\{ O_1 \ln^2\tilde{s}\frac{\sin(K_-\tilde{\tau})}{K_-\tilde{\tau}}\exp(b_{-1}t) + O_2\ln\tilde{s}\cos(K_-\tilde{\tau})\exp(b_{-2}t) + O_3\exp(b_{-3}t)\Big\}\,. \quad (18)$$

$$F_-^O(s,t) = C_O\exp(b_O t) \times \Phi_-(\alpha_O(t))(s/s_0)^{\alpha_O(t)}\,, \quad (19)$$

$$F_-^{OP}(s,t) = \frac{C_{OP}}{\ln\tilde{s}}\exp(b_{OP}t) \times \Phi_-(\alpha_{OP}(t))(s/s_0)^{\alpha_{OP}(t)}\,, \quad (20)$$

$$F_-^R(s,t) = -C_R\exp(b_R^- t) \times \Phi_-(\alpha_R^-(t))(s/s_0)^{\alpha_R^-(t)}\,, \quad (21)$$

$$F_-^{RP}(s,t) = \frac{-tC_{RP}}{\ln\tilde{s}}\exp(b_{RP}^- t) \times \Phi_-(\alpha_{RP}^-(t))(s/s_0)^{\alpha_{RP}^-(t)}\,, \quad (22)$$

$$\Phi_-(\alpha(t)) = \mathrm{i}\cos\left(\frac{\pi}{2}\alpha(t)\right) + \sin\left(\frac{\pi}{2}\alpha(t)\right), \quad (23)$$

$$\alpha_O(t) = 1 + \alpha_O' t\,, \quad (24)$$

$$\alpha_{OP}(t) = 1 + \frac{\alpha_P'\alpha_O'}{\alpha_P' + \alpha_O'} t\,, \quad (25)$$

$$\alpha_R^-(t) = \alpha_R^-(0) + \alpha_R^{-\prime} t\,, \quad (26)$$

$$\alpha_{RP}^-(t) = \alpha_R^-(0) + \frac{\alpha_P'\alpha_R^{-\prime}}{\alpha_P' + \alpha_R^{-\prime}} t\,, \quad (27)$$

O_1, O_2, O_3, K_-, b_1^-, b_2^-, b_3^-, C_O, b_O, C_{OP}, b_{OP}, C_R^-, b_R^-, C_{RP}^-, b_{RP}^-, α_O', $\alpha_R^-(0)$ and $\alpha_R^{-\prime}$ being constants.

The AGN amplitudes defined through (1)–(27), lead to an excellent description of the standard dataset:

$$\chi^2/\mathrm{d.o.f.} = 1.16 \quad (28)$$

for a total of 1966 experimental points. The σ_T and ρ data (238 experimental points) correspond to an energy range $5\,\mathrm{GeV} \le \sqrt{s} \le 1.8\,\mathrm{TeV}$. The $\mathrm{d}\sigma/\mathrm{d}t$ data (1728 experimental points) correspond to an energy range $9.3\,\mathrm{GeV} \le \sqrt{s} \le 1.8\,\mathrm{TeV}$ and to a t range $0.1\,\mathrm{GeV} \le |t| \le 2.6\,\mathrm{GeV}^2$. The presence of the maximal odderon is, of course, crucial in order to describe the experimental difference between the pp and $\bar{p}p$ differential cross sections at $\sqrt{s} = 52.8\,\mathrm{GeV}$ in the dip–shoulder region $1.1\,\mathrm{GeV} < |t| < 1.5\,\mathrm{GeV}^2$ [6,7].

Now, we generalize the AGN model by introducing the following three ingredients.

1. First we have contributions $N_\pm(s,t)$ to $F_\pm(s,t)$ behaving like t^{-4} at high t:

$$N_+(s,t) = \mathrm{i}sN_+\ln\tilde{s}\frac{-t}{(1-t/t_+)^5}\,, \quad (29)$$

$$N_-(s,t) = sN_-\ln\tilde{s}\frac{-t}{(1-t/t_-)^5}\,. \quad (30)$$

These additional terms add just four free parameters more as compared with the original AGN model. Similar forms as those of (29)–(30) were used in [8].
The experimental t^{-4} behavior at large t is well known. The theoretical motivation for $N_-(s,t)$ was given a long time ago by Donnachie and Landshoff: the odderon three-gluon exchange, with elementary gluons [9]. The motivation for $N_+(s,t)$ is more obscure, but it could be correlated with the $C = +$ part of the exchange of three elementary gluons.

2. Next, we have a crossover factor $Z_-(t)$ in the $F_-(s,t)$ amplitude:

$$Z_-(t) = \frac{\tanh(1-t/t_c)}{\tanh(1)}\,. \quad (31)$$

This factor introduces just one more free parameter as compared with the original AGN model.
The phenomenological motivation for such a $Z_-(t)$ factor is obvious: the $\bar{p}p$ and pp cross at very small t ($|t| \simeq 0.16\,\mathrm{GeV}^2$) and the respective crossover point is practically independent on s.

3. Then there are two linear functions $(1 + A_{MO}t)$ and $(1 + A_O t)$, which multiply the maximal odderon and

Table 1. The values of parameters in $F_+(s,t)$

Name	Dimension	Value	Error
H_1	mb GeV^2	0.22	0.002
H_2	mb GeV^2	−0.016	0.001
H_3	mb GeV^2	27.43	0.30
K_+		0.20	0.001
C_p	mb GeV^2	2.65	0.16
C_{PP}	mb GeV^2	−40.04	2.18
C_R^+	mb GeV^2	77.61	1.71
C_{RP}^+	mb GeV^2	−23.73	0.70
$\alpha_R^+(0)$		0.67	0.01
$\alpha_R^{+\prime}$	GeV^{-2}	0.80	0.01
α_P'	GeV^{-2}	0.41	0.01
b_{+1}	GeV^{-2}	3.06	0.03
b_{+2}	GeV^{-2}	0.66	0.01
b_{+3}	GeV^{-2}	4.57	0.03
b_P	GeV^{-2}	0.31	0.07
b_{PP}	GeV^{-2}	9.18	0.44
b_R^+	GeV^{-2}	4.80	0.14
b_{RP}^+	GeV^{-2}	0.46	0.02
N_+	mb GeV^2	−9.42	0.33
t_+	GeV^2	0.45	0.01

Table 2. The values of parameters in $F_-(s,t)$

Name	Dimension	Value	Error
O_1	mb GeV^2	0.002	0.001
O_2	mb GeV^2	0.12	0.01
O_3	mb GeV^2	−2.13	0.08
K_-		0.011	0.002
C_O	mb GeV^2	0.88	0.02
C_{OP}	mb GeV^2	0.061	0.005
C_R^-	mb GeV^2	38.00	0.37
C_{RP}^-	mb GeV^2	−4753	101
$\alpha_R^-(0)$		0.53	0.01
$\alpha_R^{-\prime}$	GeV^{-2}	0.80	0.01
α_O'	GeV^{-2}	0.10	0.01
b_{-1}	GeV^{-2}	1.07	0.02
b_{-2}	GeV^{-2}	2.87	0.06
b_{-3}	GeV^{-2}	3.09	0.04
b_O	GeV^{-2}	2.29	0.02
b_{OP}	GeV^{-2}	0.18	0.01
b_R^-	GeV^{-2}	1.42	0.05
b_{RP}^-	GeV^{-2}	8.44	0.77
N_-	mb GeV^2	2.16	0.20
t_-	GeV^2	0.61	0.01
A_{MO}	GeV^{-2}	7.32	0.32
A_O	GeV^{-2}	8.87	0.41
t_c	GeV^2	−0.16	0.004

the odderon pole contributions, respectively. These factors have also a phenomenological justification: they allow us to better describe the smallness of the odderon forward couplings at present energies. These linear functions introduce just two more free parameters as compared with the original AGN model.

In fact, we considered a big number of fits by taking into account just one additional ingredient or a combination of two additional ingredients. The net result is that, for an excellent fit of the standard dataset, we need all the three ingredients. This result is not trivial, because we add a ridiculously small number of free parameters (seven free parameters) as compared with the total of 36 free parameters of the AGN model. Moreover, we considerably increase the number of fit data points: from 1966 to 2892. Therefore, we are convinced that the three ingredients represent a safe theoretical generalization of the AGN model at high t.

The best value of the free parameters involved in the amplitudes defined in (4)–(27) and (29)–(31) with the additional three ingredients are obtained through a χ^2 MINUIT minimization and they are shown in Tables 1 and 2.

The χ^2/d.o.f. is surprisingly small:

$$\chi^2/\text{d.o.f.} = 1.23\,, \tag{32}$$

by taking into account the huge number of experimental data that are fit (2892 points) in a huge range of energies:

$$5\ \text{GeV} \le \sqrt{s} \le 1800\ \text{GeV} \tag{33}$$

and in a huge range[2] of t:

$$t = 0 \quad \text{and} \quad 0.1\ \text{GeV} \le |t| \le 16\ \text{GeV}^2\,. \tag{34}$$

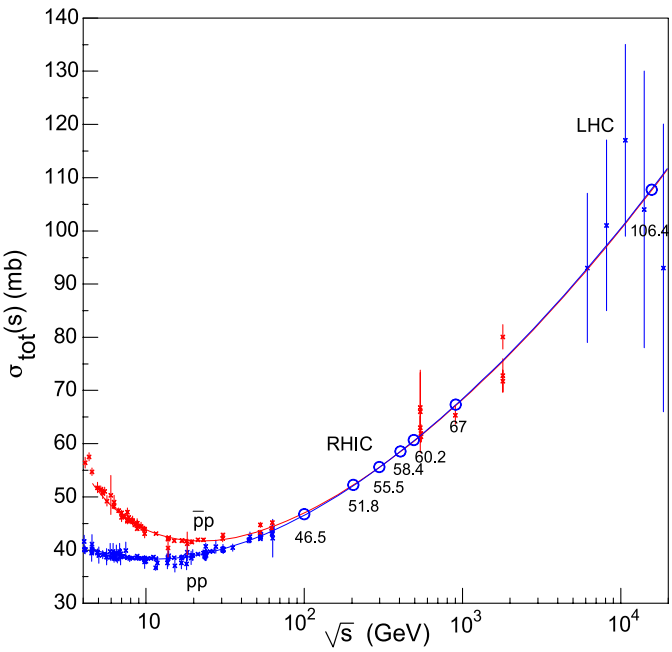

Fig. 1. Total cross sections. Our predictions at RHIC and LHC are also shown

We note that the value of χ^2/d.o.f. for $|t|$ values higher than 2.6 GeV^2 is 1.37.

[2] The range in (34) is justified in [3]. We exclude 244 points, most of them at low energies, from the dataset in [3] (corres-

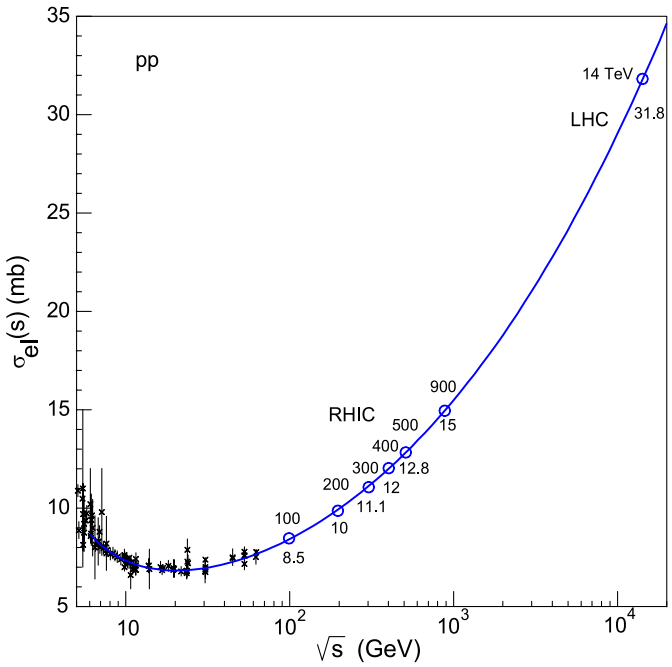

Fig. 2. pp elastic cross sections. Our predictions at RHIC and LHC are also shown

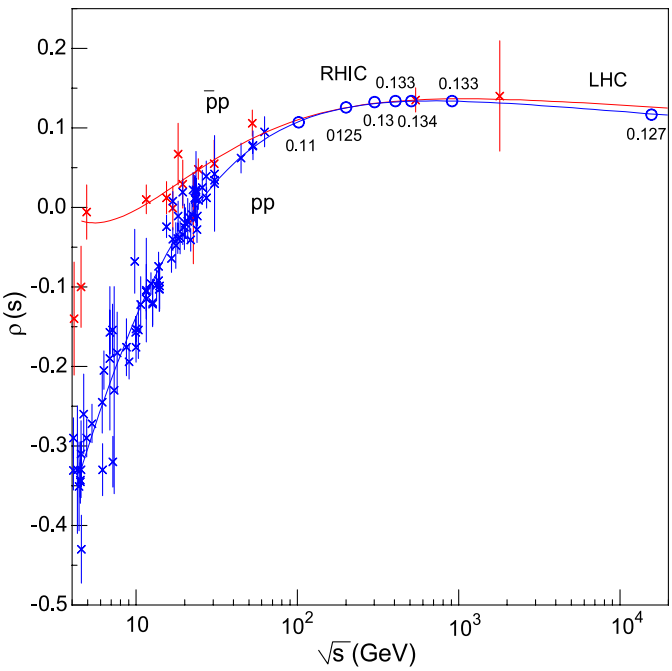

Fig. 3. ρ parameter. Our predictions for pp scattering at RHIC and LHC are also shown

The fit presented in this paper is certainly the best existing model for describing the data. We present here all our analytic forms and all the values of the parameters so any author can compare his/her own model with our model.

ponding to five pp sets and two $\bar{p}p$ sets), because they are in conflict with all the other data.

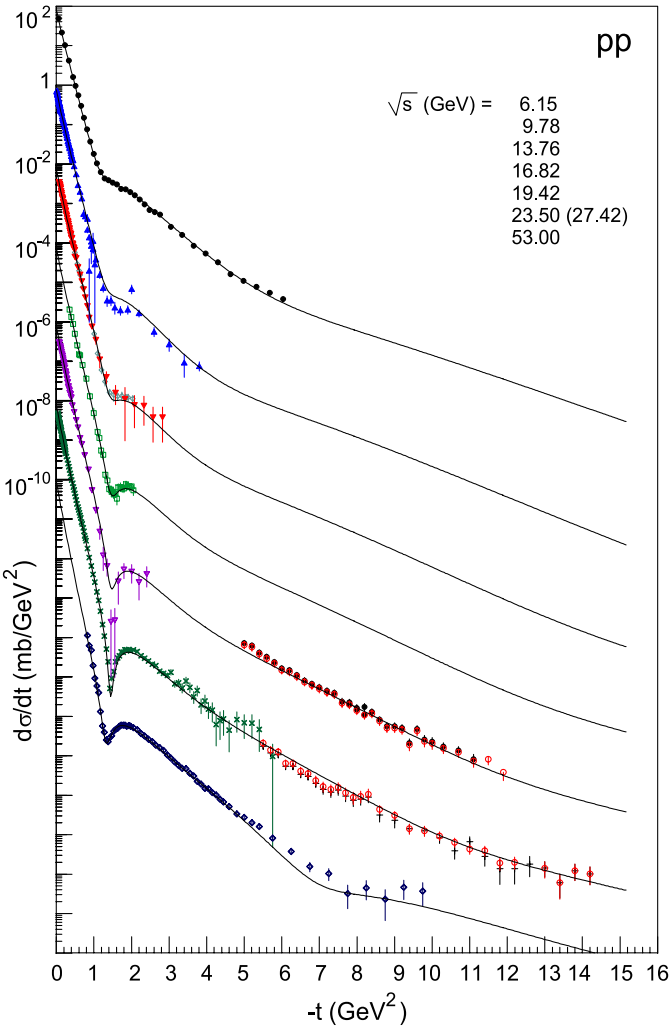

Fig. 4. pp differential cross sections in the energy range 6.15 GeV $\leq \sqrt{s} \leq$ 53 GeV. Data and theoretical values are multiplied by $10^{-2(n-1)}$, where n is the number of curve (and corresponding dataset) starting from the *top*

The quality of the fit is shown in Fig. 1 (total cross sections $\sigma_{\rm tot}(s)$), Fig. 2 (elastic cross sections $\sigma_{\rm el}(s)$), Fig. 3 (ρ parameter $\rho(s)$), Fig. 4 (pp differential cross sections), and Fig. 5 ($\bar{p}p$ differential cross sections). In Figs. 1–3 we also show our predictions for $\sigma_{\rm tot}(s)$, $\sigma_{\rm el}(s)$ and $\rho(s)$ at RHIC and LHC energies.

It is, of course, interesting to compare our fit with other existing ones.

We cannot compare our fit with the original AGN fit in the whole set of data simply because the AGN model has poles in the high-t region. The AGN model was especially built for the small-t region only.

However, we can compare our fit with those of Martynov [10] and of Avila and Menon [11].

Martynov studied elastic pp and $\bar{p}p$ scattering in models of the unitarized pomeron, and he gets $\chi^2/N = 1.51$ for pp scattering and $\chi^2/N = 1.41$ for $\bar{p}p$ scattering (where N is the respective number of experimental points for $t \leq 6$ GeV^2), to be compared with our numbers 1.19 and 1.36, respec-

tively. However, one has to note that the model of [10] has a smaller number of free parameters than our model.

It is more difficult to compare our fit with that of Avila and Menon for pp scattering, because these authors do not consider the standard set of data. In particular, they argued for a possible energy independence of pp data at high t and therefore they consider blocks of data mixing different energies. However, if we just compare our result $\chi^2/N = 1.26$ for 19 GeV $< \sqrt{s} <$ 63 GeV and $|t| > 0.1$ GeV^2 with those of Table V in [11], we see that our χ^2 value is better than that of Avila and Menon $\chi^2/N = 1.6$.

Our predictions for the pp differential cross sections at RHIC and LHC energies are shown in Fig. 6. We predict (see Fig. 6) a dip–shoulder structure persisting at RHIC and LHC energies, namely a dip at $|t| \simeq 0.7$ GeV^2 for $\sqrt{s} = 500$ GeV, which moves to $|t| \simeq 0.5$ GeV^2 for $\sqrt{s} =$ 14 TeV, while the shoulder present at $|t| \simeq 1$ GeV^2 for $\sqrt{s} =$ 500 GeV moves to $|t| \simeq 0.8$ GeV^2 at $\sqrt{s} = 14$ TeV.

In Fig. 7, we plot the slope $B_{pp}(s,t)$ of the differential cross sections at RHIC and LHC energies as a function of s *and* t. A very interesting effect can be contemplated in Fig. 7: at RHIC energies $B(s,t)$ is constant at fixed s in a quite large range of t but at LHC energies the constancy of $B(s,t)$ is totally lost: the exponential behavior of $\mathrm{d}\sigma/\mathrm{d}t$ is no more valid.

All these predictions can be verified at RHIC and LHC energies. In particular, the TOTEM experiment will explore the large-$|t|$ pp elastic scattering till 8 GeV^2 [12]. Also

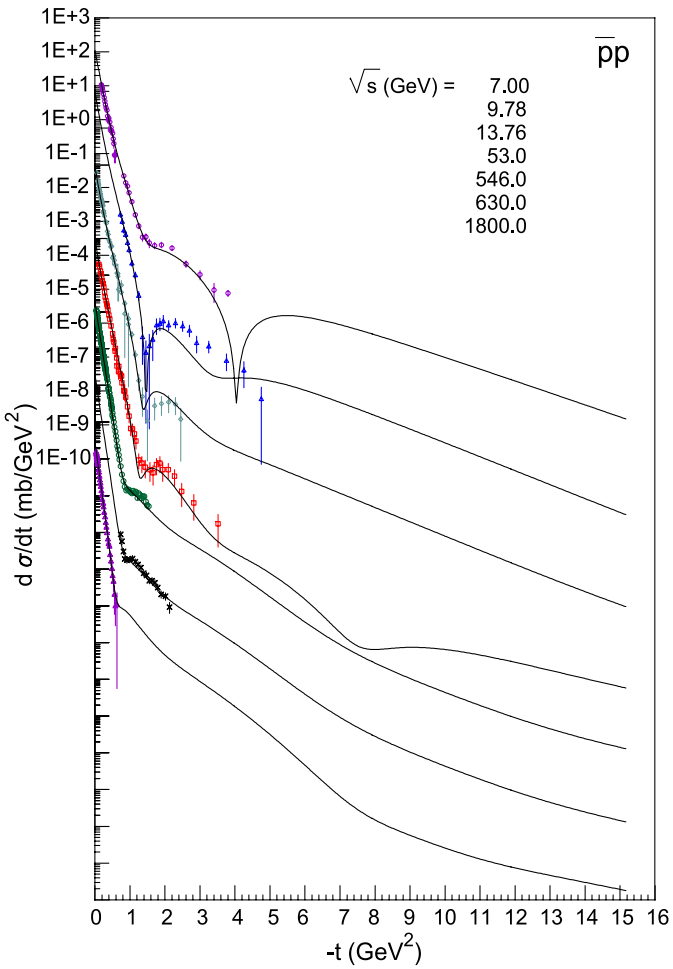

Fig. 5. $\bar{p}p$ differential cross sections in the energy range 7 GeV $\leq \sqrt{s} \leq$ 1.8 TeV. Data and theoretical values are multiplied by $10^{-2(n-1)}$, where n is the number of curve (and corresponding dataset) starting from the *top*

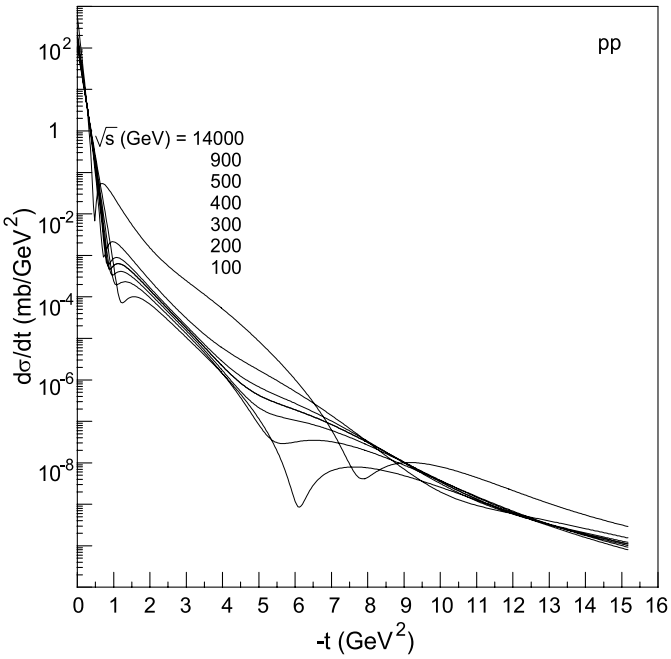

Fig. 6. Evolution of pp differential cross sections from RHIC to LHC energies

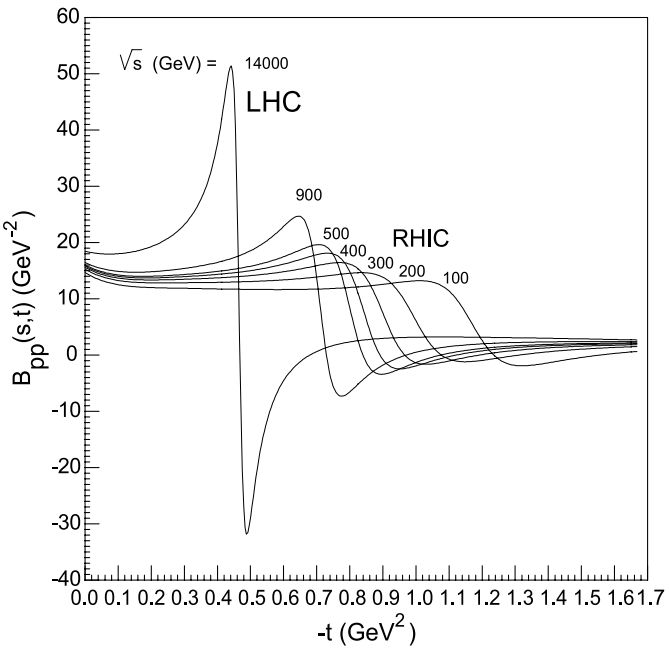

Fig. 7. Evolution of the slope in pp scattering $B_{pp}(s,t) \equiv \frac{1}{t} \ln\left(\frac{\mathrm{d}\sigma/\mathrm{d}t}{\mathrm{d}\sigma/\mathrm{d}t|_{t=0}}\right)$ from RHIC to LHC energies

experiments at RHIC will be very helpful. The verification of our predictions can help to clarify the dynamics involved in small- and high-t scattering.

Acknowledgements. We thank Prof. J.R. Cudell and Dr. P. Gauron for useful discussions. One of us (E.M.) thanks Prof. Pascal Debu for the kind hospitality at LPNHE Paris, where the present work was finished. E.M. also thanks the Ukrainian Fund of Fundamental Researches and the Department of Physics and Astronomy of National Academy of Sciences of Ukraine for a support of this work partially performed in Kiev.

References

1. R.F. Avila, P. Gauron, B. Nicolescu, Eur. Phys. J. C **49**, 581 (2007) [hep-ph/0607089]
2. B. Nicolescu, 0707.2923 [hep-ph]
3. J.R. Cudell, A. Lengyel, E. Martynov, Phys. Rev. D **73**, 034008 (2006) [hep-ph/0511073]
4. Durham Database Group, M.R. Whalley et al., http://durpdg.dur.ac.uk/hepdata/reac.html
5. http://www.theo.phys.ulg.ac.be/~cudell/data
6. A. Breakstone et al., Phys. Rev. Lett. **54**, 1280 (1985)
7. S. Erhan et al., Phys. Lett. B **152**, 131 (1985)
8. P. Desgrolard, M. Giffon, E. Martynov, Eur. Phys. J. C **18**, 359 (2000) [hep-ph/0004150]
9. A. Donnachie, P.V. Landshoff, Nucl. Phys. B **348**, 297 (1991)
10. E. Martynov, Phys. Rev. D **76**, 074030 (2007) [hep-ph/0703248]
11. R.F. Avila, M.J. Menon, 0712.3398 [hep-ph]
12. TOTEM Collaboration, K. Eggert, Proc. of the 11th International Conference on Elastic and Diffractive Scattering – Towards High Energy Frontiers, Château de Blois, France, ed. by M. Haguenauer, B. Nicolescu, J. Tran Thanh Van (Thê Giôi Publishers, Vietnam, 2006), p. 21 [hep-ex/0602025]